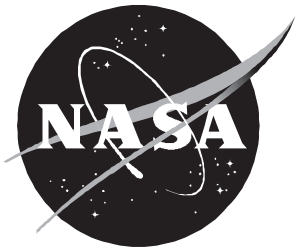

NASA Technical Memorandum 4578

Numerical Aperture Limits on Efficient Ball Lens Coupling of Laser Diodes to Single-Mode Fibers With Defocus To Balance Spherical Aberration

R. Gale Wilson

November 1994

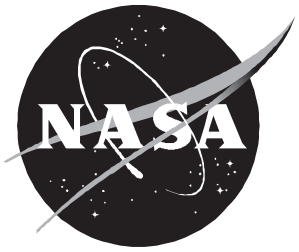

NASA Technical Memorandum 4578

Numerical Aperture Limits on Efficient Ball Lens Coupling of Laser Diodes to Single-Mode Fibers With Defocus To Balance Spherical Aberration

R. Gale Wilson
Langley Research Center • Hampton, Virginia

National Aeronautics and Space Administration
Langley Research Center • Hampton, Virginia 23681-0001

November 1994

Acknowledgment

Carl L. Fales, Jr., of NASA Langley Research Center assisted in calculating the coupling efficiencies used herein.

This publication is available from the following sources:

NASA Center for AeroSpace Information
800 Elkridge Landing Road
Linthicum Heights, MD 21090-2934
(301) 621-0390

National Technical Information Service (NTIS)
5285 Port Royal Road
Springfield, VA 22161-2171
(703) 487-4650

Summary

The potential capabilities and limitations of single ball lenses for coupling laser diode radiation to single-mode optical fibers have been analyzed; parameters important to optical fiber communications were specifically considered. These parameters included coupling efficiency, effective numerical apertures, lens radius, lens refractive index, wavelength, magnification in imaging the laser diode on the fiber, and defocus to counterbalance spherical aberration of the lens. Limiting numerical apertures in object and image space were determined under the constraint that the lens perform to the Rayleigh criterion of 0.25-wavelength units (Strehl ratio = 0.80) with defocus compensation to balance spherical aberration of the lens. The spherical aberration-defocus balance to provide an optical path difference of 0.25 wavelength units was shown to define a constant coupling efficiency (i.e., 0.56). The relative numerical aperture capabilities of the ball lens were determined for a set of wavelengths and associated fiber-core diameters of particular interest for single-mode optical fiber communication. The results support continuing efforts in the optical fiber communications industry to improve coupling links within such systems with emphasis on manufacturing simplicity, system packaging flexibility, relaxation of assembly alignment tolerances, cost reduction of optoelectronic components, and long term reliability and stability.

Introduction

There are continuing efforts to improve coupling links in optical fiber communication systems. These improvements address a variety of needs: manufacturing simplicity, system packaging flexibility to permit a single lens arrangement to accommodate a variety of applications, cost reduction of optical and optoelectronic components, relaxation of assembly alignment tolerances, efficient radiant power coupling to the fiber, long term component reliability, and long term stability under a variety of environmental conditions (refs. 1–4). Various coupling arrangements have been studied and applied, especially arrangements coupling laser diode (LD) power to a single-mode fiber (SMF) (refs. 4–12). Lenses generally compensate for the different numerical apertures (NA's) of the laser and the fiber and otherwise provide coupling compatibility between the laser and the fiber mode fields. Optimum coupling occurs when LD and SMF spot sizes are matched.

Ball lenses are one of the physically simplest and most economical micro-optic elements to fabricate and mount. These lenses, in both single and multielement assemblies, have been the subject of various investigations of methods to perform coupling tasks economically, efficiently, compactly, and without alignment complexity (refs. 4 and 12–21). These investigations have shown several potential origins of coupling inefficiency. In nearly all cases, the coupling inefficiency is dominated by the spherical aberration (SA) of the lens collecting the divergent LD radiation; reduction of the lens aberration is the primary concern in developing efficient coupling (ref. 15). Reduced coupling inefficiency is achieved with lenses of small radius (R) and high refractive index (n), because the losses due to SA decrease with decreasing R or focal length (proportional to R) and increasing n. The SA increases as larger NA's are used. Therefore, moderate coupling efficiency can be maintained with small diameter and/or high-n lenses to accommodate larger NA's associated with divergent LD source outputs. In addition, defocus can partially compensate for SA (refs. 5 and 22–24).

The study presented herein provides supplementary analyses relevant to LD to optical fiber coupling by a single ball lens, with a moderate constant coupling efficiency of 0.56 and an appropriate accounting for defocus to balance SA (fig. 1). These analyses clarify relationships among several variables pertinent to general and laboratory applications for optical fiber communications. These variables are R, NA in the object and image spaces, magnification (M) of the LD onto the fiber, wavelength (λ), n, and the LD distance (D_o) and the fiber distance (D_i) measured from the lens principal plane. While existing literature presents a variety of relationships and data, specific quantitative assessments of NA limits in terms of these variables and any particular coupling efficiency apparently have not been explicitly presented previously. In the literature, there often is ambiguity regarding the focal determination (z misalignment) in calculations and measurements of coupling efficiency. The analyses presented herein consider only the case of single ball lens coupling to the fiber, which represents one commercially available standard pigtail configuration.

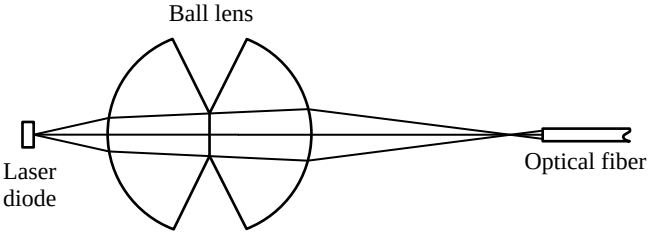

Figure 1. Laser diode to fiber coupling configuration.

Symbols and Abbreviations

D_i	fiber distance measured from lens principal plane
D_o	LD distance measured from lens principal plane
FWHM	full width at half maximum
GRIN	gradient index
LD	laser diode
M	magnification
NA	numerical aperture
n	refractive index
OPD	optical path difference
PSF	point spread function
R	ball lens radius
SA	spherical aberration
SMF	single-mode fiber
λ	wavelength

Background and Overview

For a lens with only SA, each level of SA has a unique focal shift that maximizes the coupling efficiency when the receiving fiber is placed at some new position (defocused) relative to the paraxial image surface (ref. 5). Coupling efficiencies are presented as functions of wave-front defocus aberration with wave-front SA ranging from 0 to 0.7 wavelength units (ref. 5). Maximum coupling efficiency occurs for values of defocus aberration about equal to the SA. References 23 and 24 show that SA = 1λ when balanced by an equal amount of defocus aberration produces only peak optical path difference (OPD) of 0.25λ in the pupil, which is the minimum amount tolerated within the Rayleigh criterion (Strehl ratio = 0.80) when only SA is present.

In the study presented herein, in which only SA applies (fig. 1), the results of reference 5 have been extrapolated by calculation for the case of SA = 1λ and 1λ of defocus to determine the coupling efficiency corresponding to OPD = 0.25λ. The application of equation (23) on page 2681 of reference 5 to this case gives a coupling loss of -2.5 dB (a coupling efficiency of 0.56). (See table 1.) Therefore, satisfaction of the Rayleigh criterion actually provides only a moderately high coupling efficiency. The calculations are somewhat tedious, because the coupling efficiency is expressed in terms of a Laplace transform that in turn is a function of a complementary error function with a complex argument; therefore, only the result is given.

The same analysis for a Strehl ratio = 0.90 led to an optical coupling efficiency of 0.65. The relationship between coupling efficiency and Strehl ratio > 0.90 is summarized in table 1. These data were generated from correlating the graphical data in figure 11 in reference 5 and figure 2 in reference 25. The results show that to achieve a coupling efficiency above 0.75 requires a balanced SA small enough to yield a Strehl ratio > 0.95 (i.e., a balanced SA $\approx 0.4\lambda$ or smaller and an OPD $\approx 0.1\lambda$ or less). These results seem to be restricted only to a simple optical fiber coupling configuration, such as the one in the study presented herein, in which only SA and/or misalignments contribute to coupling losses (ref. 5).

Table 1. Estimated Relationship Between Coupling Efficiency and Strehl Ratio

Coupling efficiency	Strehl ratio	Balanced SA, wavelength units[a]	OPD, wavelength units
0.56	0.80	1.0	0.25
.65	.90	.7	.18
.69	.92	.6	.15
.73	.95	.5	.13
.77	.97	.4	.10
.82	.98	.3	.08
.88	.99	.2	.05
1.00	1.00	0	0

[a] Equal to defocus wave-front aberration.

The results reported in references 11 and 26 address specifically the correction of asymmetric (noncircular or elliptic) and astigmatic outputs from LD and the reduction of beam divergence. In addition, many studies have accompanied gradient index (GRIN) lens technology developments (ref. 12) and applications to optical coupling. Molded aspheric lenses (ref. 26) incorporate the inherent advantages of aspheric over spherical surfaces in collimation, focusing, and coupling of LD beams. These advantages, which provide increased availability of LD's with improved output beams, emphasize the importance of more completely quantifying the limitations and the capabilities of the single ball lens for coupling such sources to single-mode fibers. Only by such quantification will it be possible to compare the performance of the ball lens with other more complex systems and to further clarify its potential suitability for specific simple and inexpensive applications.

The ray-trace program applied in the study reported herein supports analysis of uniform-amplitude wave fronts, whereas a LD source is more accurately described by a Gaussian-amplitude wave-front distribution. Differences between and similarities in the behavior of uniform-amplitude and Gaussian-amplitude beams have been discussed at length with laser applications in mind (refs. 27–35). The ratio of the spot sizes at any two conjugate planes in an optical system is equivalent to the geometric M between the two conjugate planes (ref. 31). For a given small amount of SA, the Strehl ratio for a pupil with Gaussian-amplitude beam distribution is somewhat higher than that for a uniformly illuminated pupil. That is, for a given Strehl ratio, a Gaussian pupil can tolerate slightly more SA than a uniform pupil (refs. 33 and 35). It appears that the results reported herein of calculations of optimized NA for a slightly aberrated uniform beam (OPD = 0.25λ) may be only slightly conservative relative to results for similar moderately aberrated Gaussian beam if the beam is accommodated within the calculated NA without significant truncation.

Analytical Methods and Approach

The imaging system of the study presented herein consists of the coupling of radiation from a LD source (object) to a SMF by a single ball lens (fig. 1). As mentioned earlier, this configuration is one commercial standard pigtail arrangement with the ball lens. The magnified diameter of the LD output beam generated at the fiber entrance aperture constitutes the image. The lens is treated as a three-surface construction with two real spherical surfaces of equal curvature but opposite sign and an artificial limiting aperture coincident with the principal (diametrical) plane.

This optical layout is consistent with that of other ball lens analyses in references 13–15, 20, and 21. The optical coupling efficiencies of these lens analyses are calculated by integrating the overlapping LD and SMF fields in the principal plane of the lens. Such an aperture stop would not physically exist in an application because the effective NA of the system would be determined by the NA limitation of the optical fibers.

All the data were generated with the Kidger Optics Ltd. MacSIGMA optical design and analysis program through the ray-tracing and diffraction-analysis modules. The program requires specification of an aperture-stop surface that is consistent with the role of pupils in optical systems analyses. For the configuration in figure 1, with essentially a point-source object, no aberrations other than spherical exist in the results obtained with MacSIGMA. The LD is assumed to be nonastigmatic, which is consistent with the more general application of index-guided LD's.

The primary emphasis of the study presented herein was to define limiting NA's for a range of lens R, λ, and M applicable to optical communications requirements (fig. 1). The limiting NA determinations were defined to satisfy the Rayleigh criterion of 0.25λ relative to the pupil OPD with defocus enhancement. These NA's also correspond to a 0.56 coupling efficiency, which was determined on the basis of only SA loss, as noted earlier.

For SMF applications, table 2 presents a guideline for matching λ and fiber-core diameter (ref. 36). Representative SMF's, as shown in table 2, have core diameters between 4.5 and 11 μm, depending on the wavelength of application. Single-mode operation depends conjunctively on the λ, the core diameter, and the n difference (step index profile) between the core and the cladding. To provide mode matching between the LD and the fiber, the M required for the optical system with a typical LD source that has a beam waist of 1 μm or a diameter of 2 μm is a number that is equal to one-half of the magnitude of the fiber core diameter (refs. 13, 20, and 21). For some n profiles and typical operating λ, the fiber mode field diameter may be slightly larger than the core diameter (ref. 37).

Table 2. Wavelength and Diameter for Optical Fiber Communications

[From ref. 36]

λ, μm	Fiber core diameter, μm
0.85	5–10
1.30	9–10
1.55	4.5–11

The limiting NA's reported herein were determined from the finite (real) ray trace and are the sines of the marginal (limiting) ray angles in the object and the image spaces. The apertures were determined for optimized defocus conditions. The fiber is positioned toward the lens and away from paraxial focus to counterbalance SA and permit performance of the lens that is consistent with the Rayleigh criterion.

For each calculation, optimized NA (object and image) and defocus were determined iteratively, with the maximum NA chosen that allowed the Rayleigh criterion to be marginally satisfied. That is, the

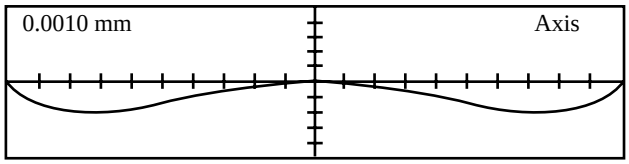

(a) Meridional scan with rays originating on axis.

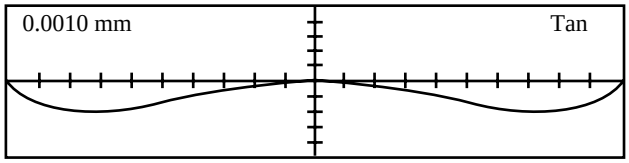

(b) Meridional scan with rays originating at edge of laser diode.

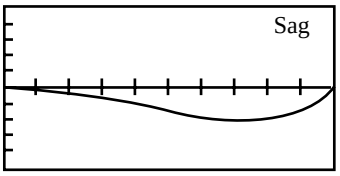

(c) Sagittal scan.

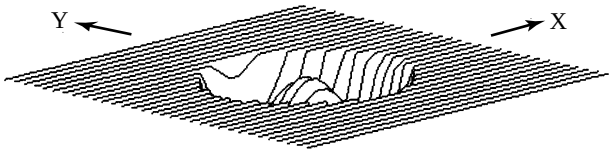

(d) Three dimensional plot of optical path difference.

Figure 2. Plots of typical optical path difference across lens exit pupil.

OPD is not allowed to exceed 0.25λ anywhere across the pupil. A balance between the defocus aberration and the SA is achieved by choosing the exit pupil OPD (wave-front aberration) to be zero at the edges (periphery) of the pupil; it is zero at the center by definition of the reference wave-front position (fig. 2). Spherical wave-front aberration varies with the fourth power of the pupil R, while defocus expressed as a wave-front aberration varies with the second power of the pupil R. Therefore, a balance at the edges of the pupil can be achieved when the peak SA and the peak defocus OPD are opposite in sign.

These optimized defocus conditions equivalently satisfy a Strehl ratio = 0.80, which represents a recognized standard of near-diffraction-limited performance for an imaging system. (See refs. 22 and 38.) For small aberrations, the Strehl ratio has a maximum value when the aberration variance has a minimum value. The best image plane corresponds to the minimum variance value, which is a balance between the peak defocus and the peak SA's that occur at the edges of the pupil (ref. 23).

In the iterative specification and calculation process, an arbitrary small tolerance about Strehl ratio = 0.80 was permitted. The final Strehl ratio values were within the range of 0.796 to 0.809. The numerical apertures referred to throughout the remainder of the paper are the optimized (maximum) values, which with proper defocus values, satisfy a Strehl ratio = 0.80. The primary interest is in enlarging the object space NA to accommodate divergent LD radiation. The detailed presentation of image space NA data is secondary to detailed presentation of the object space NA data. For very small fiber diameters (magnifications), the NA definition in terms of fiber acceptance angle, or marginal ray angle, may have limited meaning (ref. 39). That is, the geometrical optics treatment is not totally adequate to describe the modal, or wave, character of the light propagation and its Gaussian profile. Although manufacturers do not normally specify NA for SMF, optical fiber communications literature cites values from less than 0.1 to about 0.3 (refs. 36 and 40). All values of image space NA generated in the study presented herein show a general consistency with this range of values. Therefore, both the image space and the object space NA values reported herein are applicable to SMF optical communication tasks. The exception of a few values of image space NA > 0.3 will be discussed in the section entitled "Variable Refractive Index."

In the iterative process, for specific λ, R, n, and M specified for the paraxial focus, a best guess image space NA was entered in the MacSIGMA program (a NA specification is required to set up the correct aperture in image space when generating rays) and the Strehl ratio was computed for conditions of balanced SA and defocus aberration. The program then provided the corresponding object space NA. In all cases presented herein, the dimension of the LD beam diameter (object size) was specified as 2 μm; however, smaller or larger object sizes that are still small relative to the lens scale can be chosen. Lens diameters ranged from 0.075 to 3.0 mm, which corresponds to some values for commercially available products. The values of M at the paraxial image surface were also iterated for target values of true transverse M at the actual image surface (defocus

position). The true M is the ratio of the chief ray height at the image to the chief ray height at the object, or equivalently, the ratio of the actual image distance to the actual object distance. Both the image distance and the object distance are measured from the lens principal plane.

The exit pupil was sampled by a grid that provided 16 rays across the diameter of the pupil to obtain the wave-front aberration over the pupil. The point spread function (PSF) was then computed by fast Fourier transform techniques for the ball lens exit pupil and the corresponding perfect pupil; from these results, the Strehl ratio was derived. Experimentation with a sampling grid of doubled density did not produce significantly different results.

For the study described herein, it seems important to recognize the limitations of the geometrical analysis tools that have been used. The field of lens design and optical systems analysis, which uses such computer programs as MacSIGMA, is based on geometrical ray tracing with limited diffraction-analysis features (refs. 41–43). Examination of Fresnel numbers for the focused beams in the study presented herein indicates that the ray-tracing techniques should be adequate, but if smaller ball lenses were to be evaluated, the diffraction-analysis limitations of the program should be more carefully examined.

Results and Discussion

Optimized NA data for three λ's for a constant lens $n = 1.76$ as a function of M with R as a parameter is shown in figures 3(a) and (b), 4(a) and (b), and 5(a) and (b). These data cover three ranges of M; each range is appropriate for the corresponding fiber-core diameters and λ for a typical LD source with waist size (radius) of 1 μm, or a diameter of 2 μm. These ranges of M provide LD images to match fiber-core diameters of 5 to 10, 9 to 10, and 4.5 to 11 μm for the respective λ values of 0.85, 1.30, and 1.55 μm, which are relevant to optical fiber communications applications (table 1). The $n = 1.76$ at these λ's represents several materials, including sapphire and related glasses for laser applications. A more detailed discussion of the results appears in the section entitled "Constant Refractive Index."

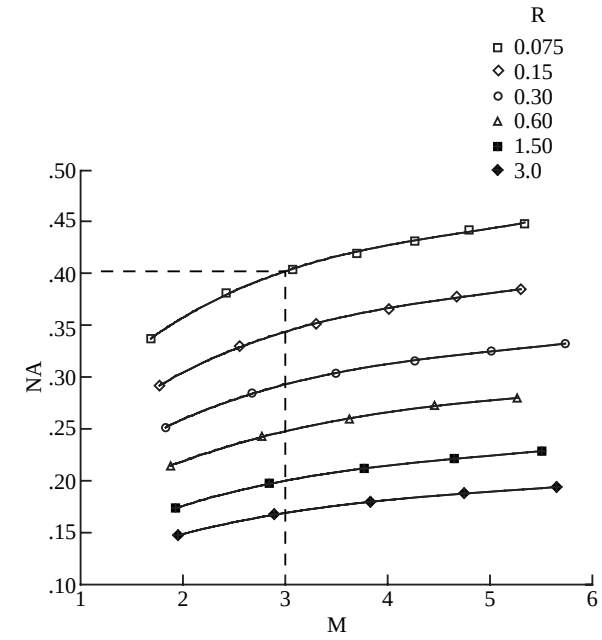

(a) Object space.

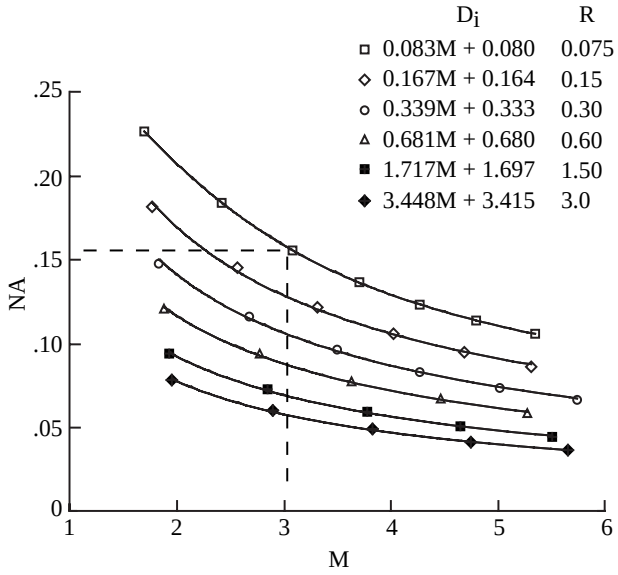

(b) Image space.

Figure 3. Dependence of NA on ball lens M of laser diode with defocus to balance SA and provide 0.25λ-OPD wave front. Coupling efficiency = 0.56; $\lambda = 0.85$ μm; $n = 1.76$.

The optimized NA dependence on lens n ($n \geq 1.76$), with λ, M, and R as parameters, is shown in figures 6(a), (b), and (c) and 7(a), (b), and (c). Boundary values of NA were established corresponding to the shortest (0.85 μm) and longest (1.55 μm) values of λ, to the highest (5.5) and lowest (2.25) values of M, to the smallest (0.075 mm) and largest (3.0 mm) lens R, and to values of n ranging from 1.76 to 3.50, which was the maximum n applicable without truncation of the lens sphere. The image space NA and defocus were iterated as necessary to satisfy a Strehl ratio = 0.80.

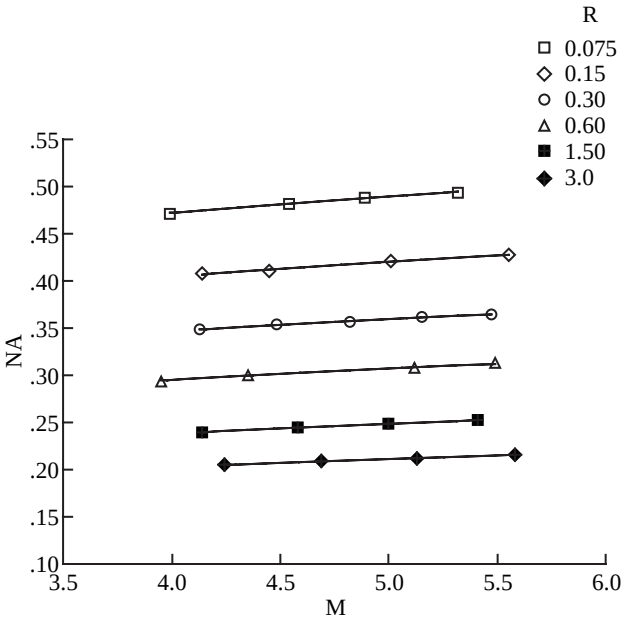

(a) Object space.

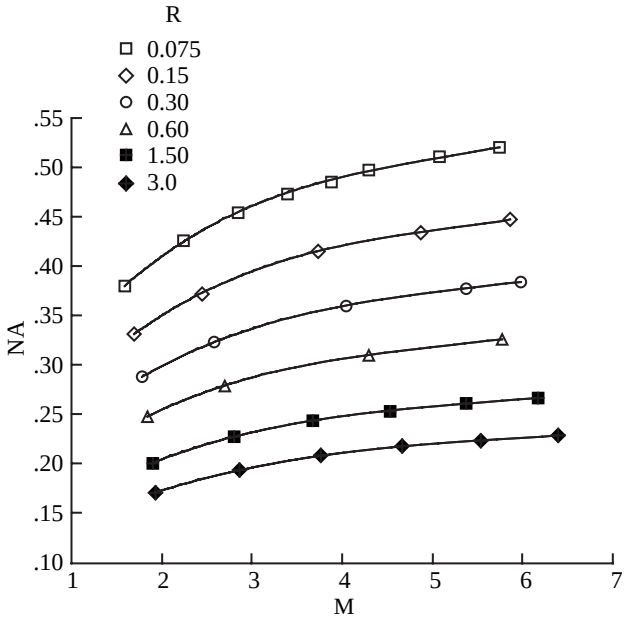

(a) Object space.

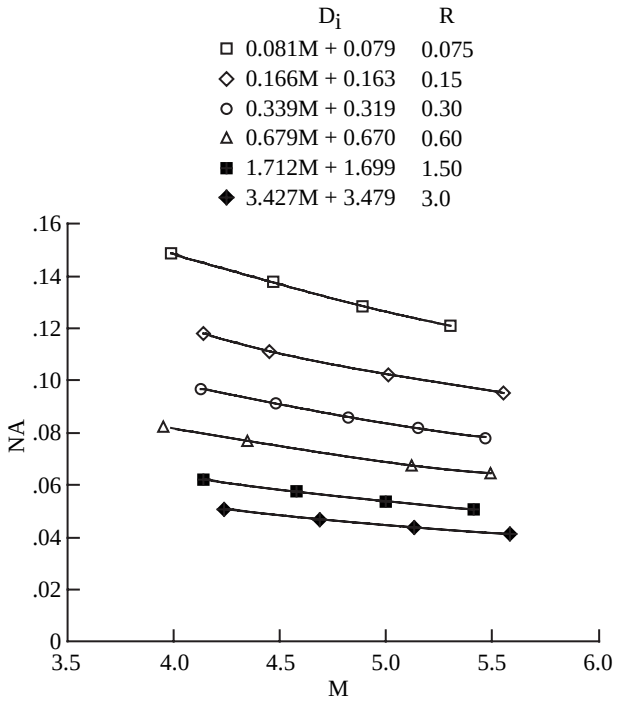

(b) Image space.

Figure 4. Dependence of NA on ball lens M of laser diode with defocus to balance SA and provide 0.25λ-OPD wave front. Coupling efficiency = 0.56; $\lambda = 1.3$ μm; $n = 1.76$.

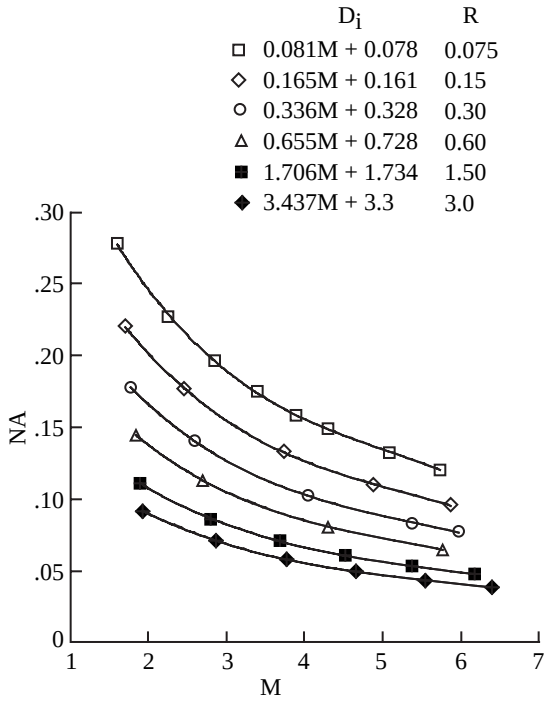

(b) Image space.

Figure 5. Dependence of NA on ball lens M of laser diode with defocus to balance SA and provide 0.25λ-OPD wave front. Coupling efficiency = 0.56; $\lambda = 1.55$ μm; $n = 1.76$.

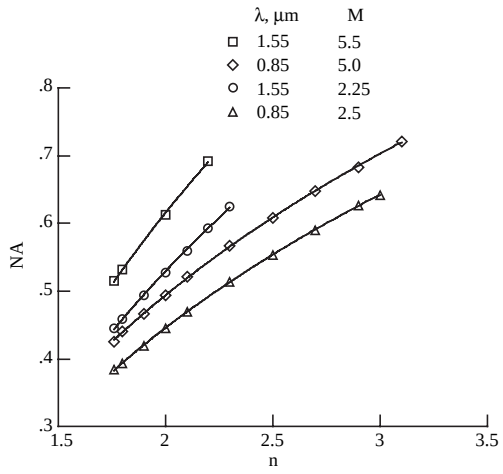

(a) $R = 0.075$.

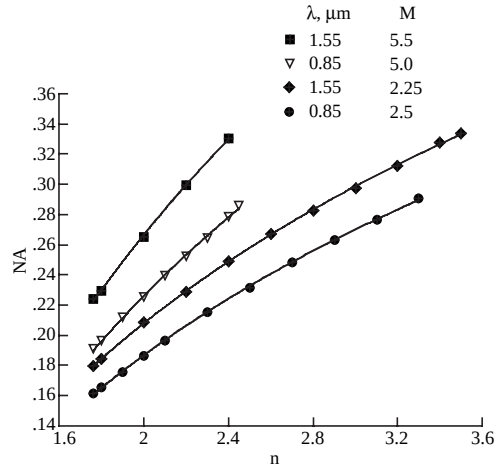

(b) $R = 3.0$.

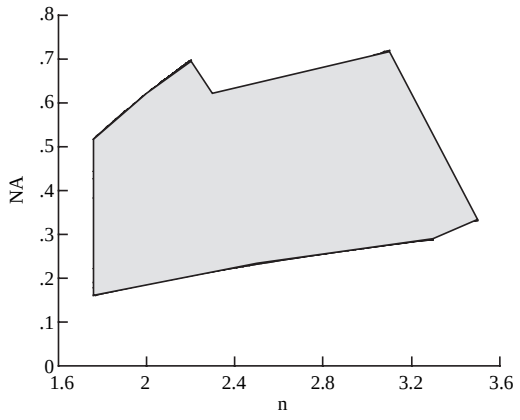

(c) Composite parameter space for $R = 0.075$ and 3.0.

Figure 6. Dependence of object space NA on n with defocus to balance SA and provide 0.25λ-OPD wave front. Coupling efficiency = 0.56.

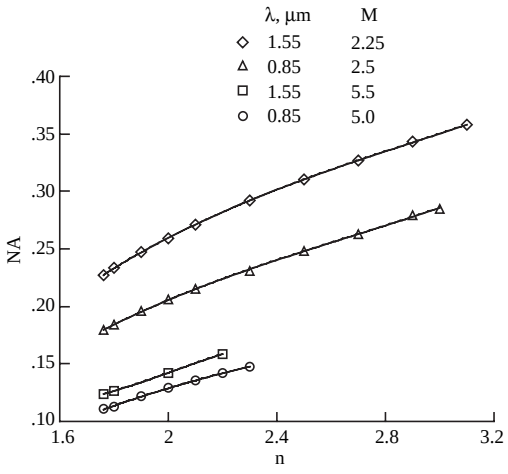

(a) $R = 0.075$.

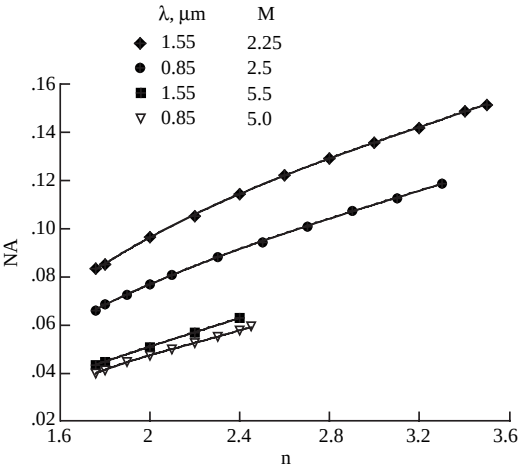

(b) $R = 3.0$.

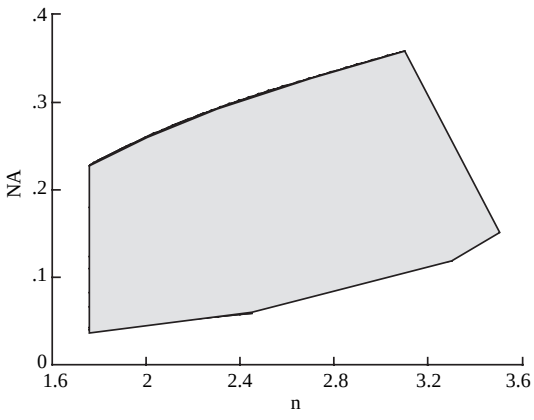

(c) Composite parameter space for $R = 0.075$ and 3.0.

Figure 7. Dependence of image space NA on n with defocus to balance SA and provide 0.25λ-OPD wave front. Coupling efficiency = 0.56.

Constant Refractive Index

Figure 3(a) presents the object space (LD) optimized NA as a function of M for $\lambda = 0.85$ μm and $n = 1.76$ with the lens R as a parameter. As expected, the highest values of NA are for the smallest lens and the smallest values correspond with the largest lens. Intermediate values of NA are found for intermediate lens R. This pattern is consistent over the range of M. The M is true transverse M at the defocus image plane. The NA for a given lens radius has a nonlinear positive dependence on M.

Within the bounds of the variables and divergence characteristics of LD's, and with coupling efficiency fixed at 0.56 and n fixed at 1.76, these data make it possible to assess the capabilities and limitations of ball lenses for LD to single-mode coupling in a variety of optical fiber communications and other applications. The divergence angle of the LD is typically defined as the full width at half maximum (FWHM) of the far-field beam irradiance, when the angle is referenced to the center of the beam at its waist. Therefore, the NA equivalent could be defined as the sine of one-half of that angle. Alternatively, the divergence angle may refer to the $1/e$ or the $1/e^2$ irradiance point. Some judgment is needed in defining the NA equivalent of the laser beam.

For purposes of discussing suggested use of the data reported herein, it will be assumed that it is desirable to couple a LD beam of known divergence (spot size) and λ to a fiber with compatible core diameter. The ball lens capabilities can be evaluated as a function of lens R and required M. For example, in figure 3(a), an optimum choice of lens for a LD with divergence angle corresponding to a NA ≈ 0.4 and $\lambda = 0.85$ μm coupled to a fiber at $M \geq 3$ would be limited to one of $R \leq 0.075$ mm. As shown in figure 3(b), which presents the counterpart image space NA data, the NA of the coupling beam at the fiber would be about 0.16 or less, depending on the M. Since the LD divergence angle and the spot size are coupled, the data should be interpreted accordingly. That is, the data can be applied to LD's with waist sizes somewhat smaller or larger than 1 μm, or to fiber mode field diameters somewhat larger than the fiber-core diameters. From MacSIGMA, it was determined that the same optimized NA results are obtained when the object size is varied from 1 to 3 μm. These results were expected since the source size is still very small relative to the lens parameters. As part of the data generation, a broadened range of M's was covered, relative to the ranges corresponding strictly to the fiber-core diameters listed in table 2.

In figure 3(b), for a given lens R, the image space NA decreases nonlinearly with increasing M. For each size lens, a linear expression for image distance as a function of M is presented in figures 3(b), 4(b), and 5(b) for the three λ. Then, the associated object distance from the lens center D_o is determined by dividing the image distance by the M.

The data of figures 4 and 5 will be discussed only briefly, since there is an exact parallel with the data in figure 3. The object space NA for the $\lambda = 1.3$ μm are presented in figure 4(a), emphasizing the range of M from 4.5 to 5.0. The behavior of NA with M is similar to that for the shorter λ, but NA for the longer λ are larger for corresponding ranges of M. The image space NA data corresponding to the data in figure 4(a) are shown in figure 4(b).

For $\lambda = 1.55$ μm, the object space NA data are presented in figure 5(a). The pattern of NA behavior with M is similar to that observed in the middle λ data. Data for image space NA corresponding with data in figure 5(a) are given in figure 5(b).

The pattern of object space NA behavior as a function of lens R for a given λ is expected because the potential coupling efficiency increases with decreasing lens R (reduced SA). For a given lens size and given M, both the object and image NA increase with increasing λ. This increase is expected because the wave-front aberration across the lens pupil becomes smaller in λ units as the λ increases. For a given lens size and a given λ, the object space NA consistently increases with M, while the image space NA decreases with M.

Variable Refractive Index

Figures 6(a), (b), and (c) display the results of studies in which the optimized object space NA was evaluated as a function of n with the smallest and largest lens R, the shortest and longest λ, and the smallest and largest M as parameters. Figures 7(a), (b), and (c) show the image space counterparts of the data in figure 6. Part (a) of figures 6 and 7 present data for lens $R = 0.075$ mm (higher NA), part (b) of figures 6 and 7 present data for $R = 3.0$ mm (lower NA), and part (c) of figures 6 and 7 present composite data of the total NA and n space determined by the boundary R, λ, and M. The lowest n value of 1.76 is the same throughout figures 6 and 7. The upper index value, however, varies among the data sets and reaches a cutoff value for each data set that is associated with the lens source when it is located a very small distance (less than or equal to about 1 percent of the lens diameter) from the first lens surface. That is, for $n > 2.0$, the lens paraxial focal

point lies inside the lens, and the object distance from the front lens surface ultimately reduces to zero with increasing values of n and M. To obtain usable larger NA would require truncating the ball lens on the object side, thus making it a plano-convex lens. As anticipated, the highest values of NA (object and image space) are associated with the smallest lens and longest λ. However, because of the interactive inputs of M, n, and lens R on optimized NA, the highest NA does not correspond with the highest n. As seen in figure 6(b), the lower boundary of object space NA values corresponds with the largest lens R, a small M value, and the shortest λ. It is observed from examining all the data at $\lambda = 0.85$ and 1.55 μm in conjunction with the data in figures 4(a) and (b) for $\lambda = 1.3$ μm that the numerical apertures at $\lambda = 1.3$ μm for all the lens radii as a function of n should be bounded by the object space data in figures 6(a) and (b) and by the image space data in figures 7(a) and (b). (See figs. 6(c) and 7(c).) However, the high-n sides of the boundary polygons in figures 6(c) and 7(c) are only drawn approximately, since NA and n data were not actually generated for the intermediate lens radii.

The behavior of the image space NA shown in figures 7(a), (b), and (c) as a function of n is similar to that for object space. The upper boundary of values of image space NA corresponds with the smallest lens R, the longest λ, and the smallest M (fig. 7(a)). The lower boundary of image space NA values (fig. 7(b)) corresponds with the largest lens R, but with a combination of λ and M. The image distance from lens center to defocus plane is not simply expressible as a function of n. Therefore, the values have been provided in table 3. As before, the LD distance is given by $D_o = D_i/M$.

A nominal practical upper value of NA for SMF has been reported as 0.3 (ref. 36). It can be seen from figure 7(b) and figure 7(c) that for $\lambda = 1.55$ μm, $R = 0.075$ mm, and $M = 2.25$, the image space NA somewhat exceeds 0.3 for the applicable larger values of n. Therefore, these data and the corresponding object space data in this relatively small parameter space may not be of practical use.

Table 3. Defocused Image Distance From Lens Principal Plane

	Image distance, mm, at—			
n	$\lambda = 0.85$, $M = 2.5$	$\lambda = 0.85$, $M = 5.0$	$\lambda = 1.55$, $M = 2.25$	$\lambda = 1.55$, $M = 5.5$
$R = 0.075$ mm				
1.76	0.287	0.492	0.261	0.527
1.80	.279	.482	.255	.514
1.90	.261	.450	.240	
2.00	.248	.429	.227	.463
2.10	.238	.412	.219	
2.20		.396		.425
2.30	.224	.384	.204	
2.40				
2.45				
2.50	.211		.193	
2.60				
2.70	.201		.185	
2.80				
2.90	.193		.179	
3.00	.189			
3.10			.174	
3.20				
3.30				
3.40				
3.50				
$R = 3.0$ mm				
1.76	12.095	20.717	11.132	22.441
1.80	11.687	20.014	10.830	21.645
1.90	10.973	18.788		
2.00	10.383	17.802	9.608	19.345
2.10	9.953	17.002		
2.20		16.338	8.818	17.832
2.30	9.215	15.789		
2.40		15.312	8.243	16.594
2.45		15.097		
2.50	8.708			
2.60			7.829	
2.70	8.312			
2.80			7.504	
2.90	7.953			
3.00			7.246	
3.10	7.691			
3.20			7.030	
3.30	7.475			
3.40			6.852	
3.50			6.773	

Concluding Remarks

Studies reported herein better define the potentials and limitations of single ball lenses for coupling laser diode radiation to single-mode fibers, particularly for optical communications applications. The lens was required to transmit a wave front that met the Rayleigh criterion of 0.25 wavelength optical path difference (Strehl ratio = 0.80) near-diffraction-limited standard for magnifications at wavelengths practicable to single-mode fiber coupling in optical communication and for a typical laser diode source with a waist size of 1 μm. The corresponding theoretical coupling efficiency was shown to be 0.56. The numerical aperture of the lens was optimized

by balancing the inherent lens spherical aberration against defocus aberration and by positioning the fiber image plane closer to the lens than the paraxial image surface. For lens refractive index of 1.76, the study presented herein provided optimized numerical aperture as a function of magnification at wavelengths of 0.85, 1.3, and 1.55 μm, with lens radii of 0.075, 0.15, 0.30, 0.60, 1.50, and 3.0 mm as parameters. For each set of values of lens radius and wavelength, a linear expression was presented for the defocused image (fiber) distance from the lens in terms of magnification. It was found that for a fixed coupling efficiency, available numerical apertures for coupling increase with decreasing lens radius and with increasing refractive index. The object space numerical aperture for a given lens radius increases with increasing magnification, while the image space numerical aperture decreases with increasing magnification.

In another part of the study, similar numerical aperture calculations were made with refractive index varying upward from the value of 1.76. This part was directed primarily at finding the numerical aperture as a function of refractive index, with the smallest and largest lens radii, the shortest and longest wavelengths, and the smallest and largest magnifications as parameters. As a result, the upper and lower boundaries of the object and image space numerical aperture were delineated for the given parameters. The numerical aperture was a nonlinear function of index of refraction for any given set of the parameters. For each set of values of lens radius, wavelength, and magnification, the image distances were tabulated and the object distances are obtained from the relationship between object distance, image distance, and magnification. From extrapolating and correlating the results of other studies, it was shown that very high coupling efficiencies (for any simple-lens on-axis coupling configuration) require very high Strehl ratios. That is, a Strehl ratio ≈ 0.97 is required to give a coupling efficiency of about 0.77. These numbers are ideal ones. It should be recognized that there may be reducing factors in a real system such as Fresnel reflection, asymmetry in the laser diode radiation, fiber-lens misalignments, roughness and shape of the lens surface, and in some laser diodes, astigmatism losses. However, means are available to minimize losses due to such factors.

From the results of the study reported herein, one can readily assess the potentials, or limitations, of ball lenses for laser diode to single-mode optical fiber coupling in a variety of optical communications applications when the laser diode beam divergence is known. With acceptable fiber defocus to counterbalance spherical aberration of the lens, assessments can be made as functions of the lens radius, the lens refractive index, the wavelength, magnification of the laser diode onto the fiber, laser diode distance from the lens, and fiber distance from the lens. The results of this study support continuing efforts in the optical fiber communications industry to improve coupling links within such systems with emphasis on manufacturing simplicity, relaxation of assembly alignment tolerances, system packaging flexibility, cost reduction of optoelectronic components, and long term reliability and stability.

NASA Langley Research Center
Hampton, VA 23681-0001
August 8, 1994

References

1. Lipson, J.; Ku, R. T.; and Scotti, R. E.: Opto-Mechanical Considerations for Laser-Fiber Coupling and Packaging. *SPIE*, vol. 554, 1985, pp. 308–312.

2. Matthews, Michael R.; MacDonald, Brian M.; and Preston, Keith R.: Optical Components—The New Challenge in Packaging. *IEEE Trans. Components, Hyb., & Manuf. Technol.*, vol. 13, no. 4, Dec. 1990, pp. 798–806.

3. Reith, Leslie A.; Mann, James W.; Andredakis, Nicholas C.; Lalk, Gail R.; and Zah, Chung-En: Single-Mode Fiber Packaging for Semiconductor Optical Devices. *IEEE Trans. Components, Hyb., & Manuf. Technol.*, vol. 13, no. 4, Dec. 1990, pp. 791–797.

4. Reith, Leslie A.; Mann, James W.; Lalk, Gail R.; Krchnavek, Robert R.; Andreadakis, Nicholas C.; and Zah, Chung-en: Relaxed-Tolerance Optoelectronic Device Packaging. *J. Lightwave Technol.*, vol. 9, no. 4, Apr. 1991, pp. 477–484.

5. Wagner, R. E.; and Tomlinson, W. J.: Coupling Efficiency of Optics in Single-Mode Fiber Components. *Appl. Opt.*, vol. 21, no. 15, Aug. 1982, pp. 2671–2688.

6. Bludau, Wolfgang; and Rossberg, Rolf H.: Low-Loss Laser-to-Fiber Coupling With Negligible Optical Feedback. *J. Lightwave Technol.*, vol. LT-3, no. 2, Apr. 1985, pp. 294–302.

7. Honmou, H.; Ishikawa, R.; Ueno, H.; and Kobayashi, M.: 1.0 dB Low-Loss Coupling of Laser Diode to Single-Mode Fibre Using a Planoconvex Graded-Index Rod Lens. *Elec. Lett.*, vol. 22, no. 21, Oct. 1986, pp. 1122–1123.

8. Kato, Kuniharu; and Nishi, Isao: Low-Loss Laser Diode Module Using a Molded Aspheric Glass Lens. *IEEE Photonics Technol. Lett.*, vol. 2, no. 7, July 1990, pp. 473–474.

9. Shiraishi, Kazuo: New Scheme of Coupling From Laser Diodes to Single-Mode Fibers: A Beam Expanding Fiber With a Hemispherical End. *Appl. Opt.*, vol. 29, no. 24, Aug. 1990, pp. 3469–3470.

10. Stone, J.; Burrus, C. A.; and Centanni, J. C.: Long-Working Distance Expanded-Beam Fibre Microlenses. *Elec. Lett.*, vol. 27, no. 7, Mar. 1991, pp. 592–593.

11. Snyder, James J.; Reichert, Patrick; and Baer, Thomas M.: Fast Diffraction-Limited Cylindrical Microlenses. *Appl. Opt.*, vol. 30, no. 19, July 1991, pp. 2743–2747.

12. Wu, Huey-Daw; and Barnes, Frank S., eds.: *Microlenses—Coupling Light to Optical Fibers*. IEEE Press, 1991.

13. Karstensen, H.: Laser Diode to Single-Mode Fiber Coupling With Ball Lenses. *J. Opt. Commun.*, vol. 9, no. 2, 1988, pp. 42–49.

14. Hillerich, Bernd: Influence of Lens Imperfections With LD and LED to Single-Mode Fiber Coupling. *J. Lightwave Technol.*, vol. 7, no. 1, Jan. 1989, pp. 77–86.

15. Sumida, Masatoyo; and Takemoto, Kenji: Lens Coupling of Laser Diodes to Single-Mode Fibers. *J. Lightwave Technol.*, vol. LT-2, no. 3, June 1984, pp. 305–311.

16. Tamura, Yasuaki; Maeda, Hidenari; Satoh, Norikazu; and Katoh, Ken: Single-Mode Fiber WDM in the 1.2/1.3 μm Wavelength Region. *J. Lightwave Technol.*, vol. LT-4, no. 7, July 1986, pp. 841–845.

17. Nicia, A. J. A.: An Optical Communication System With Wavelength-Division Multiplexing and Minimized Insertion Losses. *Philips Tech. Review*, vol. 42, no. 8/9, June 1986, pp. 245–261.

18. Nicia, A. J. A.; Potters, C. J. T.; and Tholen, A. H. L.: An Optical Communication System With Wavelength-Division Multiplexing and Minimized Insertion Losses. *Philips Tech. Review*, vol. 43, no. 11/12, Dec. 1987, pp. 344–368.

19. Kishimoto, Ryozo; Sumida, Mesatoyo: Design for SMF Laser Diode Module Using Thick Lens. *Electron. & Comm. in Japan*, Part 2, vol. 71, no. 7, 1988, pp. 56–64.

20. Karstensen, Holger; Frankenberger, Rudolf: High-Efficiency Two Lens Laser Diode to Single-Mode Fiber Coupler With a Silicon Plano Convex Lens. *J. Lightwave Technol.*, vol. 7, no. 2, Feb. 1989, pp. 244–249.

21. Karstensen, Holger; and Drögemüller, Karsten: Loss Analysis of Laser Diode to Single-Mode Fiber Couplers With Glass Spheres or Silicon Plano-Convex Lenses. *J. Lightwave Technol.*, vol. 8, no. 5, May 1990, pp. 739–747.

22. Welford, W. T.: *Aberrations of Optical Systems*. Adam Higler Ltd., 1986.

23. Mahajan, Virendra N.: *Aberration Theory Made Simple*. Volume TT 6, SPIE—The International Society for Optical Engineering, 1991.

24. Smith, Warren J.: *Modern Optical Engineering—The Design of Optical Systems*. McGraw-Hill, Inc., 1990.

25. Mahajan, Virendra N.: Strehl Ratio for Primary Aberrations: Some Analytical Results for Circular and Annular Pupils. *J. Opt. Soc. America*, vol. 72, no. 9, Sept. 1982, pp. 1258–1266.

26. Bennett, Carole L.; and Fitch, Mark A.: Molded Aspheric Lenses. *The Photonics Design and Applications Handbook*, Laurin Publishing Co. Inc., 1992, pp. 278–280.

27. Steier, William H.: The Ray Packet Equivalent of a Gaussian Light Beam. *Appl. Opt.*, vol. 5, no. 7, July 1966, pp. 1229–1233.

28. Givens, M. Parker: Focal Shifts in Diffracted Converging Spherical Waves. *Opt. Comm.*, vol. 41, no. 3, Apr. 1982, pp. 145–148.

29. Carter, William H.: Focal Shift and Concept of Effective Fresnel Number for a Gaussian Laser Beam. *Appl. Opt.*, vol. 21, no. 11, June 1982, pp. 1989–1994.

30. Self, Sidney A.: Focusing of Spherical Gaussian Beams. *Appl. Opt.*, vol. 22, no. 5, Mar. 1983, pp. 658–661.

31. Herloski, Robert; Marshall, Sidney; and Antos, Ronald: Gaussian Beam Ray-Equivalent Modeling and Optical Design. *Appl. Opt.*, vol. 22, no. 8, Apr. 1983, pp. 1168–1174.

32. Hermann, R. M.; Pardo, John; and Wiggins, T. A.: Diffraction and Focusing of Gaussian Beams. *Appl. Opt.*, vol. 24, no. 9, May 1985, pp. 1346–1354.

33. Herloski, Robert: Strehl Ratio for Untruncated Aberrated Gaussian Beams. *J. Opt. Soc. America A*, vol. 2, no. 7, July 1985, pp. 1027–1030.

34. Kuttner, Paul: Image Quality of Optical Systems for Truncated Gaussian Laser Beams. *Opt. Eng.*, vol. 25, no. 1, Jan. 1986, pp. 180–183.

35. Mahajan, Virendra N.: Uniform Versus Gaussian Beams: A Comparison of the Effects of Diffraction, Obscuration, and Aberrations. *J. Opt. Soc. America A*, vol. 3, no. 4, Apr. 1986, pp. 470–485.

36. Yeh, Chai: *Handbook of Fiber Optics—Theory and Applications*. Academic Press, Inc., 1990.

37. Neumann, E. G.: *Single-Mode Fibers—Fundamentals*. Springer-Verlag, 1988.

38. Gaskill, Jack D.: *Linear Systems, Fourier Transforms, and Optics*. John Wiley & Sons, 1978.

39. Senior, John M.: *Optical Fiber Communications—Principles and Practice*. Prentice-Hall, Inc., 1985.

40. Palais, Joseph C.: *Fiber Optic Communications*. Prentice-Hall, Inc., 1984.

41. Lawrence, George N.; and Moore, Kenneth E.: Integration of Geometrical and Physical Optics. *SPIE*, vol. 1415, 1991, pp. 322–329.

42. Lawrence, George N.; and Moore, Kenneth E.: Optical Design and Optimization With Physical Optics. *SPIE*, vol. 1354, 1990, pp. 15–22.

43. Lawrence, George N.: Optical Design With Physical Optics Using GLAD. *SPIE*, vol. 1354, 1990, pp. 126–135.

REPORT DOCUMENTATION PAGE

Form Approved
OMB No. 0704-0188

1. AGENCY USE ONLY *(Leave blank)*	2. REPORT DATE	3. REPORT TYPE AND DATES COVERED
	November 1994	Technical Memorandum

4. TITLE AND SUBTITLE
Numerical Aperture Limits on Efficient Ball Lens Coupling of Laser Diodes to Single-Mode Fibers With Defocus To Balance Spherical Aberration

5. FUNDING NUMBERS
WU 586-03-11-11

6. AUTHOR(S)
R. Gale Wilson

7. PERFORMING ORGANIZATION NAME(S) AND ADDRESS(ES)
NASA Langley Research Center
Hampton, VA 23681-0001

8. PERFORMING ORGANIZATION REPORT NUMBER
L-17340

9. SPONSORING/MONITORING AGENCY NAME(S) AND ADDRESS(ES)
National Aeronautics and Space Administration
Washington, DC 20546-0001

10. SPONSORING/MONITORING AGENCY REPORT NUMBER
NASA TM-4578

11. SUPPLEMENTARY NOTES

12a. DISTRIBUTION/AVAILABILITY STATEMENT
Unclassified–Unlimited

Subject Category 74

12b. DISTRIBUTION CODE

13. ABSTRACT *(Maximum 200 words)*

The potential capabilities and limitations of single ball lenses for coupling laser diode radiation to single-mode optical fibers have been analyzed; parameters important to optical communications were specifically considered. These parameters included coupling efficiency, effective numerical apertures, lens radius, lens refractive index, wavelength, magnification in imaging the laser diode on the fiber, and defocus to counterbalance spherical aberration of the lens. Limiting numerical apertures in object and image space were determined under the constraint that the lens perform to the Rayleigh criterion of 0.25-wavelength (Strehl ratio = 0.80). The spherical aberration-defocus balance to provide an optical path difference of 0.25 wavelength units was shown to define a constant coupling efficiency (i.e., 0.56). The relative numerical aperture capabilities of the ball lens were determined for a set of wavelengths and associated fiber-core diameters of particular interest for single-mode fiber-optic communication. The results support general continuing efforts in the optical fiber communications industry to improve coupling links within such systems with emphasis on manufacturing simplicity, system packaging flexibility, relaxation of assembly alignment tolerances, cost reduction of opto-electronic components, and long term reliability and stability.

14. SUBJECT TERMS
Numerical aperture; Ball lens; Fiber-optic coupling; Single-mode fiber; Spherical aberration; Coupling efficiency; Defocus; Optical fiber communication

15. NUMBER OF PAGES
12

16. PRICE CODE
A03

17. SECURITY CLASSIFICATION OF REPORT	18. SECURITY CLASSIFICATION OF THIS PAGE	19. SECURITY CLASSIFICATION OF ABSTRACT	20. LIMITATION OF ABSTRACT
Unclassified	Unclassified	Unclassified	